Hydraulic bore interaction with a column - A comparison between the solution of the shallow equation and experimental results

Xinsheng Qin xsqin@uw.edu
Kaspar Mueller kasparm@uw.edu

March 13, 2015

Abstract

In this paper we compare the solution of the shallow water equations with experimental results. The experiment simulates the interaction between an incident bore and a free-standing coastal structure. The shallow water equations are solved using the GeoClaw solver of the CLAWPACK software.

We simulate and compare three different cases. In the first case we performe and evaluate a simple dam break problem. We compare the history of the wave height and velocity at the center location, where the column will be mounted. In the second case we add a square column and compare wave height at various locations in front of and behind the column. For the third case we replace the square column by a cylindrical column and compare the same variables with the experimental results. We analyze and discuss the discrepancy between the GeoClaw simulation and the experimental results.

1 Introduction

The aim of this work is to compare computational results using CLAWPACK with experimental results. This is done for the interaction of a bore and a free-standing coastal structure. The experimental results are given by Halldór Árnason [1]. We model the water using the shallow water equations, which will be introduced in Section 2. We solve these equations using CLAWPACK's GeoClaw solver, which is specialized for geophysical flow problems. In Section 3 we show how GeoClaw solves the shallow water equations and how it handles the topography. In Section 4 we describe the setup of the test case. We focus on three cases. First we compare wave height and velocity for the pure dambreak without structure in the domain in Section 5. Second we add a square column and compare wave height upstream as well as downstream of the column in 6. Lastly in Section 7 we compare the wave height at the same location but for a cylindrical column. We close this paper with a conclusion in Section 8.

2 The shallow water equations

We write the 2D depth averaged shallow water equations as

$$h_t + (uh)_x + (vh)_y = 0 \tag{1}$$

$$(hu)_t + (huv)_y + (hu^2 + \frac{1}{2}gh^2)_x = -ghB_x - Du \tag{2}$$

$$(hv)_t + (huv)_x + (hv^2 + \frac{1}{2}gh^2)_y = -ghB_y - Dv \tag{3}$$

where u, v are the horizontal depth averaged velocities, B the topography and D the drag coefficient. g denotes the gravitational acceleration. In the present case the topography will be flat except the column located downstream. The drag coefficient D is given by

$$D = \frac{gM^2\sqrt{(u^2+v^2)}}{h^{5/3}} \tag{4}$$

where M is the Manning coefficient which is $M = 0.015$. The Manning coefficient is an empirical coefficient that includes the roughness of the surface. The initial condition is given by a jump in the water depth h. The water is initially at rest.

3 The Algorithm in CLAWPACK/GeoClaw

We solve the shallow water equations with CLAWPACK. Specifically, we used the GeoClaw solver, which used a special version of the f-wave approach described in [2]. This solver combines the qualities of the Roe solver, HLLE-type solver and the f-wave approach. From the Roe solver it has the quality of giving an exact solution for a single-shock Riemann problem. Like the HLLE solver this method is depth positive semidefinite. The method has also a natural entropy-fix and gives a better approximation for problems with large rarefactions. The solver also maintains a large class of steady states. The topography and drag term are incorporated in the Riemann problem. Stability and accuracy are improved by solving a transverse Riemann problem, where the waves moving normal to the cell are split into traverse direction.
In more detail, we have the 2D hyperbolic system

$$q_t + A(q,x,y)q_x + B(q,x,y)q_y = 0 \tag{5}$$

with the wave propagation algorithm

$$\begin{aligned} Q_{ij}^{n+1} &= Q_{ij}^n - \frac{\Delta t}{\Delta x}\left(\mathcal{A}^+\Delta Q_{i-1/2,j}^n + \mathcal{A}^-\Delta Q_{i+1/2,j}^n\right) - \frac{\Delta t}{\Delta y}\left(\mathcal{B}^+\Delta Q_{i,j-1/2}^n + \mathcal{B}^-\Delta Q_{i,j+1/2}^n\right) \\ &- \frac{\Delta t}{\Delta x}\left(\tilde{F}_{i+1/2,j}^n - \tilde{F}_{i-1/2,j}^n\right) - \frac{\Delta t}{\Delta y}\left(\tilde{G}_{i,j+1/2}^n - \tilde{G}_{i,j-1/2}^n\right) \end{aligned} \tag{6}$$

In the f-wave approach the flux is decomposed the following way

$$f(Q_i) - f(Q_{i-1}) = \sum_{p=1}^{m} \mathcal{Z}_{i-1/2}^p = \sum_{p=1}^{m} \beta_{i-1/2}^p r_{i-1/2}^p \tag{7}$$

where we write this in one dimensional form, since one dimensional Riemann solvers are used. Instead of waves $\mathcal{W}$ representing the jump in Q we have now waves $\mathcal{Z}$ representing jumps in the flux. The fluctuations are defined as

$$\mathcal{A}^- \Delta Q_{i-1/2} = \sum_{p:s^p_{i-1/2}<0} \mathcal{Z}^p_{i-1/2} \quad \text{and} \quad \mathcal{A}^+ \Delta Q_{i-1/2} = \sum_{p:s^p_{i-1/2}>0} \mathcal{Z}^p_{i-1/2} \tag{8}$$

Roe eigenpairs are chosen to include the property of the Roe solver. The augmented vector is then split to provide more than $m = 2$ waves, since approximating a transonic rarefaction with a single wave can produce non-physical entropy violating numerical solutions. For the shallow water equations we have then:

$$\begin{bmatrix} H_i - H_{i-1} \\ HU_i - HU_{i-1} \\ \varphi(Q_i) - \varphi(Q_{i-1}) \\ B_i - B_{i-1} \end{bmatrix} = \sum_{p=0}^{3} \alpha^p_{i-1/2} w^p_{i-1/2} \tag{9}$$

where $\varphi(q) = (hu^2 + \frac{1}{2}gh^2)$ is the momentum flux and B_i and B_{i-1} are cell-averaged approximations of the bathymetry of the respective cell. The second and third component of $\alpha^p_{i-1/2} w^p_{1-1/2}$ are chosen to ensure conservation. These components define $\mathcal{Z}^p_{i-1/2}$. Including the $H_i - H_{i-1}$ splitting allows to create updating fluctuations that corresponds to using a depth positive semidefinite Riemann solver. For the details we refer to [2].

In the GeoClaw solver, adaptive mesh refinement (AMR) can be used. Multiple levels can be used where the domain is specified for each level. The topography for the problem is defined in a file. The topography goes into the shallow water equations through the right hand side B. The values from the file are converted into cell averages using a picewise bilinear function that interpolates the pointwise values. B is then obtained by evaluating the exact integral of this function over the cell.

4 The setup of the test case

The benchmark experiment was conducted in a 16.6 m long, 0.6m wide and 0.45 m deep wave tank. When a gate is lifted, it generates a single bore to impinge on the column located downstream. We are going to simulate 2 cases in the experiment. In the first case a bore is generated and propagates in the tank without the column. In the 2nd case a bore is generated to impinge on the column with one side facing the flow.

In the 1st case, wave height and streamwise velocity, U, at different depths, where the center of column should be located, are measured. In the 2nd case, the wave height in front of and behind the column is measured.

In all cases below, all boundary conditions are set to reflecting walls.

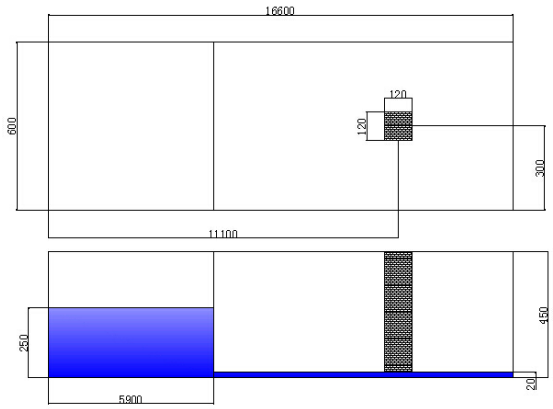

Figure 1: Diagram of experiment apparatus

5 Dam Break

The initial condition for this and the following cases is given by

$$h_0(x,y) = \begin{cases} 0.25 & x < 5.9 \\ 0.02 & \text{otherwise} \end{cases} \tag{10}$$

$$u_0(x,y) = 0 \tag{11}$$

In this comparison we will include results from OpenFOAM, an open source CFD software modeling air and water using the Navier-Stokes equations with turbulence model.

If we analyze the Rankine-Hugoniot condition of the initial conditions (10) and (11) for the shallow water equations:

$$s(h_* - h) = h_* u_* - hu \tag{12}$$

$$s(h_* u_* - hu) = hu_*^2 - hu^2 + \frac{1}{2} g(h_*^2 - h^2) \tag{13}$$

we see that we can not find a s that satisfies both equations, since u and $u*$ are zero. This means the Rankine-Hugoniot condition is not satisfied and we expect a right and left going wave originating form the dam break. Figure 2a shows the time history of the wave height, measured at the center location where the column will be mounted in the following cases. The result from GeoClaw agrees quite well in general. If we zoom in Figure 2a for smaller time range from $t = 3s$ to $t = 4s$, we get Figure 2b. In Figure 2b, GeoClaw accurately predicted the arrival of the shock at t=3.8s. The arrival time of peak predicted by GeoClaw is almost the same as that from experiment (only about 0.02 second earlier). GeoClaw overestimates the peak water level a little, while OpenFOAM gives a better value. At a later time, the wave gets reflected at the right wall of the tank, which can be seen by the second jump in wave height. GeoClaw also predicts the arrival time for this peak quite well, but overestimates the peak value by a small amount.

Figure 3 shows the time history of the streamwise velocity u from GeoClaw and experiment. Note that this velocity u in both GeoClaw and experiment are depth-averaged. GeoClaw

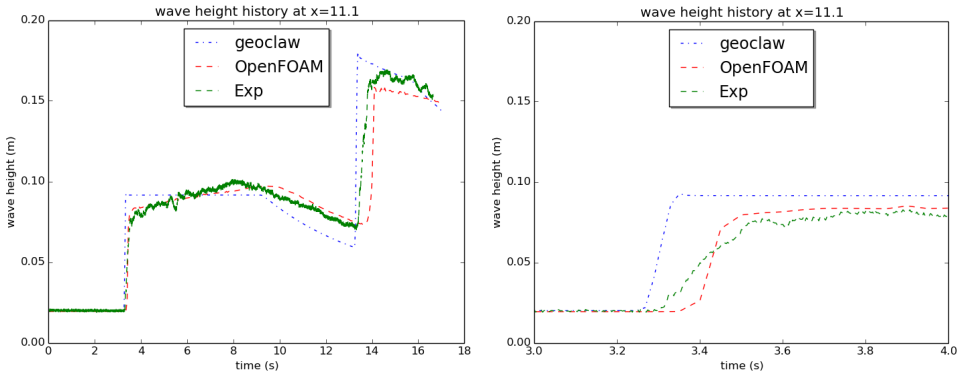

(a) time from 0 to 18 (b) time from 3 to 4

Figure 2: time history of wave height for case without a column.

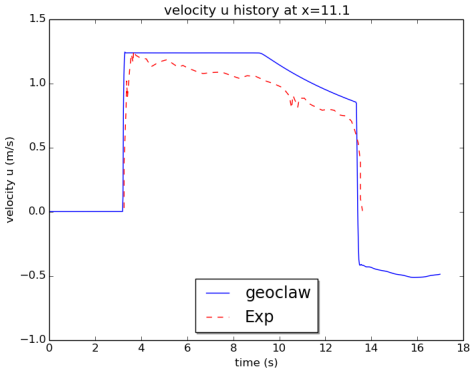

Figure 3: time history of streamwise velocity U for case without a column

accurately predicted the time of the velocity peak as well as the value of the peak. After the initial jump in the velocity, GeoClaw overestimated the value of velocity. The reason why GeoClaw gives a higher velocity may be attributed to its depth-averaged property: water at all depth are propagating with the same speed. In the experiment, the velocity is getting smaller the closer we get to the bottom.

6 Dam Break with square column

Figure 4a gives a comparison of the time history of the wave height, measured at $0.04m$ ahead of the front face of the square column($0.1m$ ahead of center of the column). There are two jumps in the result given by GeoClaw: a first jump with a change in water level from around 0.02 to 0.1 and a second jump from 0.1 to a higher level of around 0.22. If we recall from Figure 2a that the wave height is around 0.1, we can confirm that this first jump is caused by the shock wave originating from the dambreak. The second jump represents the wave reflected by the column. If we compare the time interval from the first to the second jump between measurement location $x = 11.0$ in Figure 4a and location 11.02 in Figure 4b we can see that as we get closer to the column, this time interval gets shorter.

There are two distinct differences between the GeoClaw and the experimental results. (1)In the experiment, the dambreak causes a smooth increase in water height. (2)The arrival time of the peak predicted by GeoClaw is about 0.08 seconds ahead of the time measured in the experiment.

The difference in shock shape can be explained by the difference between the shallow water equations that GeoClaw solves and the real physics of fluid. In shallow water equations, fluid viscosity is not taken into account, while in real physics it is significant. This causes the shock to retain its shape as it propagates in case of the shallow water equation, while in the experiment the shock smooths out. Thus we see a jump in the result from the shallow water equation, instead of a smooth increase as in the experimental result.

The time interval in no-column case is much smaller than that in Figure 4a, though data are not measured at exactly the same point for this two plots. This difference indicates that the column gives more resistance to shock waves in experiment than it does in shallow water equation model.

A simple analysis to this phenomenon is drawn as below. The shallow water equations are essentially a system of hyperbolic PDEs. The solution depends on initial condition along characteristics in the spatio-temporal domain. Thus, before the propagating shock arrives, all water downstream the shock has zero velocity. In other words, it does not know there is a column before the shock hits the column. This can be verified by checking the history of the wave height measured at exactly the same location, $0.04m$ ahead of the leading edge of the square column, but in different cases, one with a square column and one without. This comparison is showed in Figure 5a. As we expected, there is no difference in arrival time of the shock wave. By contrast, the Navier-Stokes equations, which better describe the real physics, are a system of PDEs of parabolic type. In real physics, or in Navier-Stokes equations, when front of the shock wave gets close to the column, water downstream it and upstream column are affected (have nonzero velocity) and resist the comming of wave to some extent. In real world this slows down the propagation speed of the shock wave when it comes close to the column and thus shifts the peak toward later time in the plots.

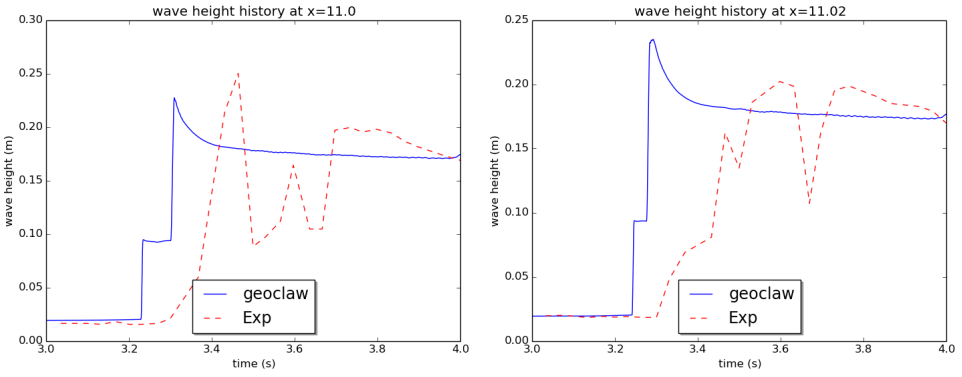

(a) at x = 11.0 (0.04m ahead of front face of the square column)

(b) at x = 11.2 (0.02m ahead of front face of the square column)

Figure 4: time history of wave height for case with a square column.

Figure 5b shows the time history of the wave height measured at the front face of the square

column. The difference between the arrival time of the peak still exists as expected. After the peak arrives, the wave gradually becomes stable as indicated by a horizontal line in the plot. In this region the differences between GeoClaw and experiment are quite small.

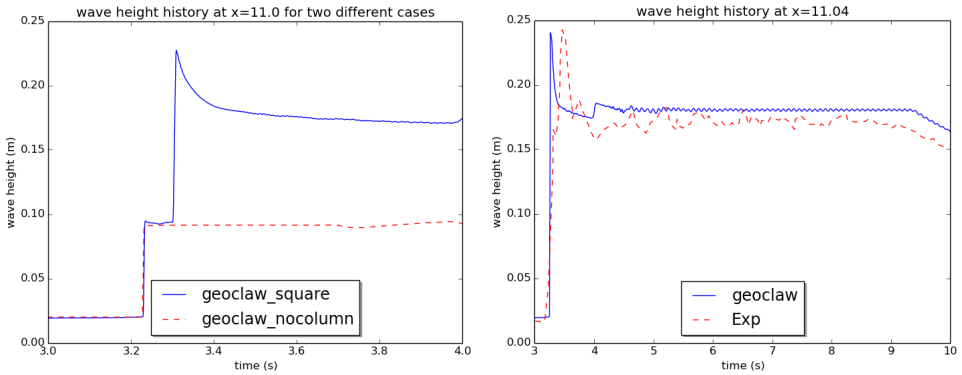

(a) comparison between case with a square column and case without one

(b) case with a square column with a larger time range at x = 11.04

Figure 5: time history of wave height for square column case

Figure 6 shows history of wave height measured at back face of the square column (at $X = 11.16$). Boundary layer detached near this region thus fluid in this region is difficult to predict. GeoClaw overestimates wave height in this region.

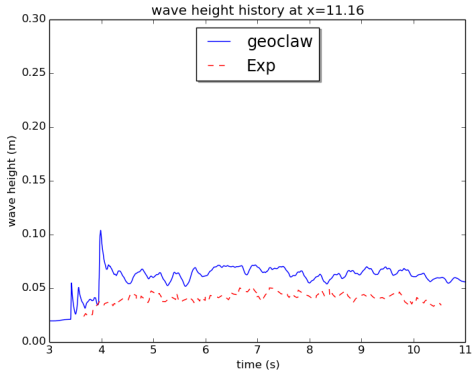

Figure 6: history of wave height measure at back face of the square column

7 Dam Break with cylindrical column

Figure 7a shows the time history of the wave height measured at $0.04m$ ahead of the front point of cylindrical column($0.1m$ ahead of the center of the column). Similar feature as in the square column case Figure 4a can be found. We can see a decrease in peak value for this case compared with the same plots for square column case. However, this decrease between two cases from GeoClaw is not as large as that between two cases from experiment.

Note that diameter of the cylinder is equal to half the length of the square column. Thus in experiment, the square column can block the flow in in a more efficient way than cylinder does, since the cylinder has a smoother shape for the fluid to pass by. This explains why we see a lower peak of wave height, as well as less steep curve for history of wave height in the case with the cylinder in the experiment. In GeoClaw, a geometry is represented with quadrilateral cells. In the cylinder case, the cylinder is represented with square cells since our background mesh is simple structured quadrilateral mesh with square cells. Based on this, we can say that in GeoClaw, when the shock wave hits the cylinder, it is hitting onto many small faces vertical to the flow direction at different locations. In other words, there is no cell which has a normal vector of front face pointing toward oblique direction other than the direction the fluid comes. Thus, it is similar to hitting onto one big face vertical to the flow direction, which is the case with a square column. This is why we get similar results in GeoClaw for the case with square column and the case with a cylinder. Figure 4a also gives results after we refine the mesh. As the mesh becomes finer, the peak value decrease as we expect. But with a even finer mesh, we cannot decrease the peak value, which indicates that a mapped grid could be used to improve the solution.

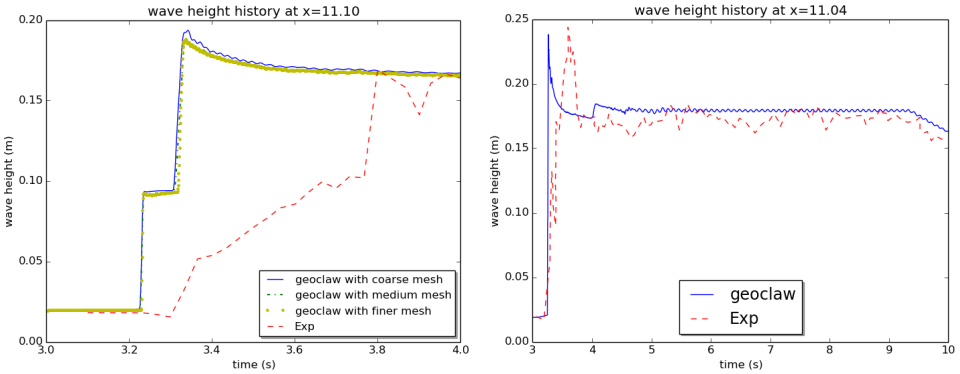

(a) at x = 11 (b) at x = 11.04

Figure 7: time history of wave height for cylindrical column case

Figure 8 shows history of wave height measured at back face of the cylinder column (at $X = 11.16$). GeoClaw gives a satisfactory prediction in this region.

Figure 7b shows the time history of the wave height for the cylinder case. As we expect, the peak predicted by GeoClaw appears earlier but the peak values agree quite well with the experiment. After the peak, GeoClaw gives a satisfactory prediction of the wave height.

8 Conclusion

In this work we compared numerical solutions of the shallow water equations using CLAWPACK's GeoClaw solver with experimental results. We saw that GeoClaw underestimates the arrival time of the shock by only 0.02s. This is in the same range as OpenFOAM predicts the arrival time. The shape of the wave although differs from the experiment and prediction from OpenFOAM. Independent of the case the arrival time is predicted always the same in GeoClaw

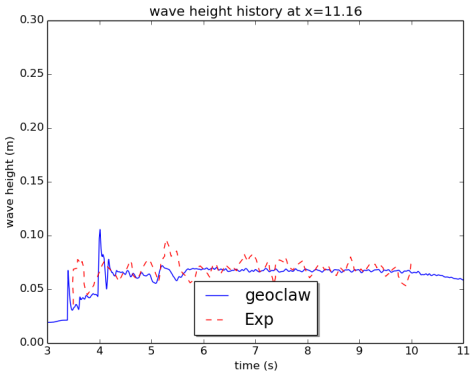

Figure 8: history of wave height measure at back face of the square column

where in the experiment the wave seems to slow down by a small amount if there is an obstacle. These discrepancies have to do with the hyperbolic character of the shallow water equations, missing turbulence model as well as depth averaging. In general GeoClaw agrees well with the measured water levels at various locations for the square as well as the cylindrical column. In the case of the cylindrical column a mapped grid could be used to improve the solution, since in the present case the cylinder shape is approximated by a quadrilateral grid. This work could also be extended by comparing the forces on the structure by using $F = \frac{1}{2} C_D \rho d h u^2$.

References

[1] Halldór Árnason (2005). Thesis - Interactions between an incident bore and a free-standing coastal structure. `http://faculty.washington.edu/cpetroff/Halldor%20dissertation.pdf`

[2] David L. George (2008) Journal of Computational Physics - Augmented Riemann solvers for the shallow water equations over variable topography with steady states and inundation.

[3] Marsha J. Berger and David L. George and Randall J. LeVeque and Kyle T. Mandli (2011) Advances in Water Resources - The GeoClaw software for depth-averaged flows with adaptive refinement.